Possible signatures of magnetic phase segregation in electron-doped antiferromagnetic $CaMnO_3$

J. J. Neumeier
Department of Physics, Florida Atlantic University, Boca Raton, Florida 33431

J. L. Cohn
Department of Physics, University of Miami, Coral Gables, Florida 33124

(Received 17 December 1999)

Specimens of the form $Ca_{1-x}La_xMnO_3$ ($0 \leqslant x \leqslant 0.2$) are utilized to study the effect of electron doping on the magnetic saturation moment M_{sat}(5 K). The systematic behavior of M_{sat}(5 K) vs x is understood through a phenomenological model which suggests the existence of local ferromagnetic regions within the antiferromagnetic host for $0.03 < x < 0.08$.

The 3*d* transition-metal oxides exhibit amazing physical effects such as high-temperature superconductivity and colossal magnetoresistance (CMR). An unusually strong interplay among charge, spin, lattice, and even orbital degrees of freedom is currently under consideration as the source for the unusual physical properties.[1–11] This interplay can cause expulsion of the doped charge carriers from antiferromagnetic regions to ordered (or unordered) lattice sites[1,6] thereby creating multiple magnetic and/or electronic phases in manganese, nickel, copper, and other transition-metal oxides. The significance of this type of phase segregation is currently the subject of a debate that could eventually provide a unifying theme under which these important oxides may be understood. Theory reveals a natural tendency for phase segregation into regions with different charge densities and magnetic states.[6–10] The coexistence of phases is familiar in nature, such as in the liquid-vapor region of phase diagrams, but in the oxides it occurs on a mesoscopic scale in a solid and over a large temperature range. In the case of CMR-related compounds, experimental investigations reveal charge ordering as well as the coexistence of antiferromagnetic (AFM) and ferromagnetic (FM) order in the form of dynamic FM correlations or magnetic droplets.[3,5,6]

The existing experimental work on CMR-related compounds has not provided detailed doping studies of low electron/hole-doping regimes and placed little emphasis on the $CaMnO_3$ region of the $Ca(La)MnO_3$ phase diagram. The present study addresses this by focusing on the addition of small electron concentrations to $CaMnO_3$ through substitution of La^{3+} for Ca^{2+}. $CaMnO_3$, being less prone to chemical defects than $LaMnO_3$,[12] is ideal for detailed doping studies. The magnetic ground state in this doping regime is commonly referred to as canted AFM, which is difficult to distinguish from a phase-segregated FM-AFM system. Careful investigation of the saturated magnetization at 5 K and a phenomenological model suggest the coexistence of multiple magnetic phases including a narrow region between 3% and 8% La doping where each doped electron ferromagnetically aligns one Mn moment, indicating that local FM regions, or FM polarons,[13] exist in the AFM environment. Electrical transport illustrates a strong correlation between the magnetic properties and electron mobility. This work reveals a unique experimental/phenomenological approach for studying weakly doped magnetic systems and introduces a potentially ideal system for in-depth experimental investigations of phase segregation and FM polarons.

All specimens were synthesized under identical conditions to minimize variations attributable to chemical defects.[12] Stoichiometric quantities of (99.99% purity or better) $CaCO_3$, La_2O_3, and MnO_2 were weighed and mixed in an agate mortar for 7 min followed by reaction for 20 h at 1100 °C. The specimens were reground for 5 min, reacted for 20 h at 1150 °C, reground for 5 min, reacted for 20 h at 1250 °C, reground for 5 min, reacted for 46 h at 1300 °C, reground for 5 min, pressed into pellets, reacted for 17 h at 1300 °C and cooled at 0.4 °C/min to 30 °C. Powder x-ray diffraction revealed no secondary phases and iodometric titration, to measure the average Mn valence, indicates the oxygen content of all specimens falls within the range 3.00 ± 0.01. Magnetic measurements were conducted with a superconducting quantum interference device magnetometer. Measurements of the electrical resistivity utilized a four-probe dc technique.

Representative magnetization M versus temperature data are presented in Fig. 1 for $Ca_{1-x}La_xMnO_3$ ($x = 0$, 0.02, 0.04, and 0.06) at 4000 Oe. $CaMnO_3$ ($x = 0$) exhibits an antifer-

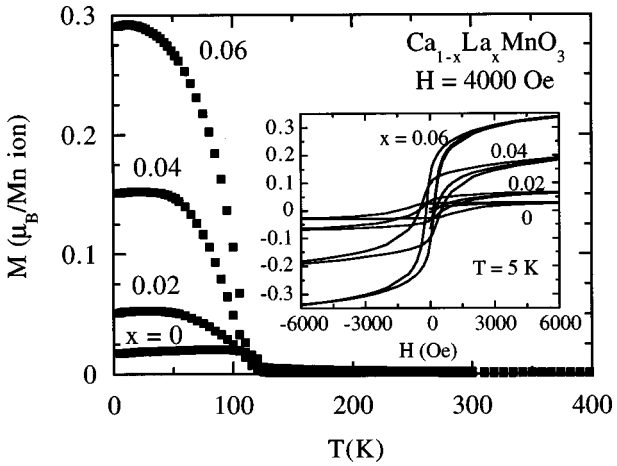

FIG. 1. Magnetization M versus temperature for $Ca_{1-x}La_xMnO_3$ ($x = 0$, 0.02, 0.04, and 0.06) at 4000 Oe. In the inset, M versus H is plotted.

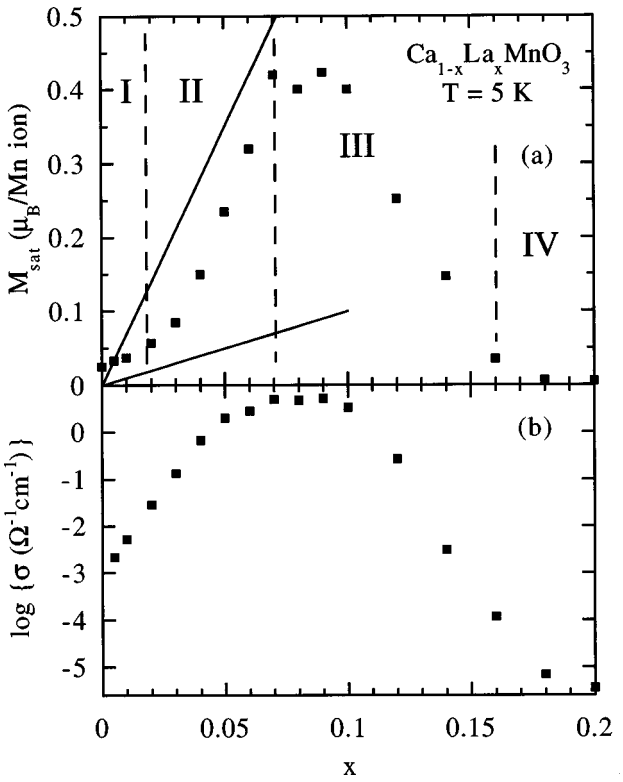

FIG. 2. (a) Magnetic saturation moment at 5 K versus La doping x. Region **I** contains G-type AFM and local ferrimagnetism. Region **II** contains local FM regions and G-type AFM. Region **III** contains C-type AFM, G-type AFM, and local FM. Region **IV** is C-type AFM. The solid lines are given by Eqs. (1) and (2). (b) Electrical conductivity σ at $T=5$ K versus x.

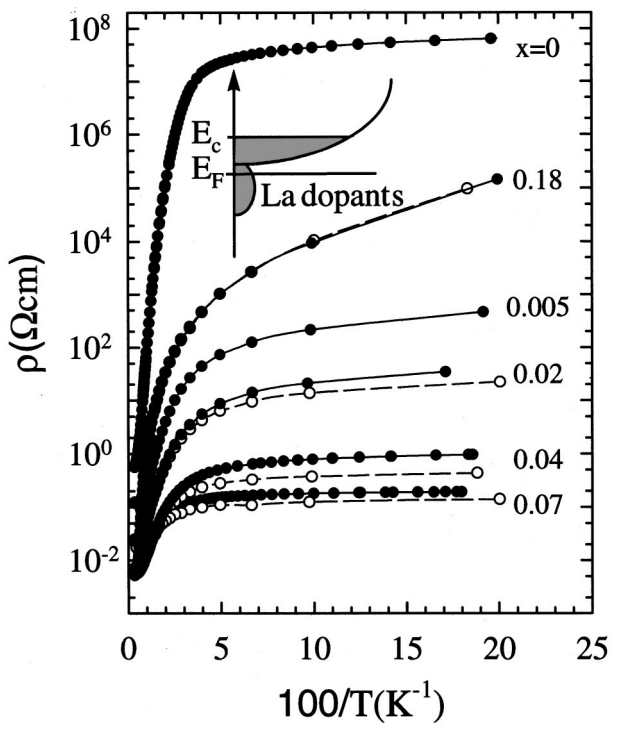

FIG. 3. Electrical resistivity at $H=0$ (solid circles) and 2 T (open circles) versus inverse temperature. The schematic band scheme shows localized states (shaded) below a mobility edge, E_C.

romagnetic transition at $T_N=131$ K with a small ferromagnetic moment resulting from a minor defect concentration. In the inset, M versus applied magnetic field H at 5 K is plotted for the same specimens. Saturation of M is indicative of ferromagnetic order. Similar observations have been made[14] in $Ca_{1-x}Bi_xMnO_3$, $Ca_{1-x}Eu_xMnO_3$, and $Ca_{1-x}Sm_xMnO_3$. Straight lines are drawn through the linear portion of the low-field M versus H data and the linear portion of the high-field region, the intercept of these two lines is defined as $M_{sat}(5\,\mathrm{K})$, the saturation moment at 5 K. To investigate the doping dependence of $M_{sat}(5\,\mathrm{K})$, it is plotted versus x in Fig. 2(a) which is equivalent to plotting the data versus electron concentration per unit cell. $M_{sat}(5\,\mathrm{K})$ versus x reveals four distinct regimes. In the region $x<0.02$, the data are nearly linear in x with a slope of $1.20\pm0.25\mu_B$/Mn-ion-electron. In the range $0.03\leqslant x\leqslant 0.08$ the data are again nearly linear, but with a much larger slope of $8.40\pm0.35\mu_B$/Mn-ion-electron. Beyond $x=0.07$, $M_{sat}(5\,\mathrm{K})$ saturates and later decreases with x finally reaching zero for $x\geqslant 0.16$.

The electron mobility is strongly correlated with $M_{sat}(5\,\mathrm{K})$ as shown in Fig. 2(b) where the $T=5$ K electrical conductivity is plotted versus x. The electrical resistivity, $\rho(T)$, is typical of heavily doped, n-type semiconductors, with three regimes evident in Fig. 3. For $T>200$ K and $0.005\leqslant x\leqslant 0.16$, a degenerate behavior with positive temperature coefficient $(d\rho/dT)$ is observed indicating that the chemical potential is positioned in the conduction band. At intermediate temperatures $(150\,\mathrm{K}\leqslant T\leqslant 50\,\mathrm{K})$, ρ $\propto\exp(E/k_BT)$ with $E\approx 85$ meV for $x=0$, $E\approx 30$ meV and nearly independent of x for $0.005\leqslant x\leqslant 0.10$, and $E\approx 85-95$ meV for $0.12\leqslant x\leqslant 0.20$. The intrinsic band gap for $CaMnO_3$ is ≈ 0.4 eV,[15] thus E is attributed to thermal activation of charge carriers from impurity states associated with chemical defects $(x=0)$ and La dopants $(x>0)$ to extended states in the conduction band. At the lowest temperatures $(T<10\,\mathrm{K})$ the activation energy is substantially smaller and doping dependent. The thermoelectric power of these samples,[16] like in the Sm-doped compounds,[14] tends to zero as $T\rightarrow 0$ indicating a finite density of states at the Fermi level. Thus, the low-temperature activation energy ε is associated with carrier hopping between localized states. The qualitative band scheme that emerges (Fig. 3, inset) is that of a conduction band tail with states localized due to the random potential introduced by the dopants up to a mobility edge E_C; this band scheme is similar to that of rare-earth magnetic semiconductors which exhibit CMR.[17] A negative magnetoresistance is observed for $H=2$ T (open symbols in Fig. 3) in the low-T regime at $x\leqslant 0.12$, but the slopes $\varepsilon=d\ln\rho/d(1/T)$ are independent of field, indicating that the applied field does not significantly increase the overlap of neighboring potential wells associated with the localized states. This is sensible since the ratio of the magnetic energies $kT_N/\mu H\approx 30$ (where μ is the magnetic moment on a Mn site).

The $M_{sat}(5\,\mathrm{K})$ data in the region $0\leqslant x\leqslant 0.07$ can be interpreted with a very simple model based on two limiting cases. Note that the AFM structure of $CaMnO_3$ is G-type, that is, each Mn magnetic moment is oriented antiparallel with regard to its nearest Mn neighbor.[2] The first case assumes that a doped electron is localized on a single Mn site with a mobility small enough to preclude double-exchange

effects, thereby creating a local Mn^{3+} moment that retains its original orientation. If we assume the orbital angular momentum is quenched, the Mn^{3+} moment has a spin $S_{3+}=2$ and an orientation opposite to that of the surrounding Mn^{4+} moments which have spin $S_{4+}=3/2$; this leads to inequivalent magnetic sites in a localized region, or a *local ferrimagnetic* region that coexists with the AFM background. Magnetization measurements would yield a net ferromagnetic saturation moment per manganese ion for such a system that, at $T=0$, would be given by

$$M_{\mathrm{sat}}(0\ \mathrm{K})=g(S_{3+}-S_{4+})\mu_B x=\mu_B x, \tag{1}$$

where g is the Landé g factor [$g=2$ (Ref. 18)] and μ_B is the Bohr magneton. Equation (1) is depicted by the lower solid line in Fig. 2(a), the slope of which is in good agreement with the observed slope of $1.20\pm0.25\mu_B$/Mn-ion-electron in region **I** ($0<x<0.02$) of Fig. 2(a). Essentially, in this limit the AFM order remains unaltered by the addition of electrons. The resulting AFM domains will possess a net magnetic moment that will rotate to the applied field direction thereby exhibiting hysteresis in M versus H as observed in the inset of Fig. 1.

In the second case it is assumed that the increased doped-electron mobility (discussed above) allows ferromagnetic coupling between two neighboring Mn moments via double-exchange[4] thereby causing a single Mn moment per doped electron to flip its orientation from AFM to FM. To calculate $M_{\mathrm{sat}}(0\ \mathrm{K})$ expected in this scenario, imagine removing n Mn^{4+} moments from an AFM lattice consisting of N Mn^{4+} moments, this would result in a net ferromagnetic moment per manganese ion of $M_{\mathrm{sat}}(0\ \mathrm{K})=g(3/2)\mu_B(n/N)$. If instead of removing the Mn^{4+} moments, their spin orientation were flipped 180°, we would obtain $M_{\mathrm{sat}}(0\ \mathrm{K})=g(6/2)\mu_B(n/N)$. The addition of the strongly Hund's coupled mobile electron, provides the final result for the net ferromagnetic saturation moment per manganese ion as a function of $x=n/N$

$$M_{\mathrm{sat}}(0\ \mathrm{K})=g(7/2)\mu_B x. \tag{2}$$

Equation (2) is plotted in Fig. 2(a) as the upper solid line; its slope of $7\mu_B$/(Mn-ion-electron) is slightly smaller than the slope of $8.40\pm0.35\mu_B$/(Mn-ion-electron) observed in region **II** ($0.03<x<0.08$) of Fig. 2(a). This discrepancy can be attributed to participation of the previously ferrimagnetic sites in the local ferromagnetism. Thus, the data in region **II** suggest that *local ferromagnetic* regions, or FM polarons, exist within the AFM lattice with one polaron created for each additional electron. Equation (2) is identical to the low-temperature limit for M_{sat} predicted[13] in a theory of polarons. We note that a minor defect concentration shifts the data in Fig. 2(a) at low x slightly upward and that the linear portion of $M(H)$ above M_{sat} is likely a result of field-induced growth of the local FM regions.

The region $0.08\leqslant x\leqslant 0.20$ reveals a saturation and suppression of $M_{\mathrm{sat}}(5\ \mathrm{K})$ resulting from the formation of *C*-type AFM regions. The *C*-type structure, known to exist at $x=0.2$,[2] is composed of one-dimensional chains of parallel magnetic moments oriented antiparallel to their neighbors suggesting double-exchange interactions along the chains and superexchange interactions between neighboring chains[19] (an example of orbital ordering). Our data suggest the doped electrons are randomly distributed among the ferromagnetic chains since $M_{\mathrm{sat}}(5\ \mathrm{K})=0$ at $x=0.2$. Furthermore, the region $x\geqslant 0.16$ is predominantly *C*-type AFM phase since $M_{\mathrm{sat}}(5\ \mathrm{K})\approx 0$ [region **IV** in Fig. 2(a)]. In the range $0.07<x<0.16$ the behavior of M_{sat} versus x indicates the coexistence of local *C*-type magnetic order with the *G*-type/local ferromagnetic mixture; this region is denoted as **III** in Fig. 2(a). Apparently, when the doped electron density becomes too high, local *C*-type regions are formed; in fact, local fluctuations in electron (or La) density may partly explain why the data in region **II** of Fig. 2(a) remain slightly below the value predicted by Eq. (2). The T_N values for $x=0.16$ and 0.18 (155 and 180 K, respectively) are significantly higher than T_N for *G*-type AFM (Fig. 1) indicating a lower free energy for the orbitally ordered *C*-type AFM phase.

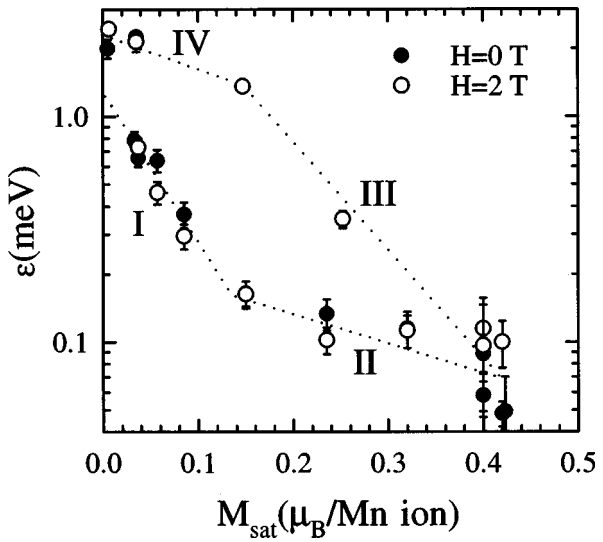

FIG. 4. Low-temperature activation energies for $\rho(T)$ at $H=0$ (solid symbols) and 2 T (open symbols) versus $M_{\mathrm{sat}}(5\ \mathrm{K})$, indicating four regimes delineated by differing slopes (lines are guides).

The different magnetic character of the four phases evidenced in Fig. 2(a) should influence the magnetic contribution to the low-T carrier hopping energy ε, thereby reflecting the difference in magnetic energy between FM clusters and the AFM background. The $\rho(x,T)$ and $M_{\mathrm{sat}}(x)$ data allow us to plot in Fig. 4 the magnetization dependence of ε in applied magnetic fields $H=0$ and 2 T. The four magnetic regimes revealed in $M_{\mathrm{sat}}(x)$ are clearly reflected as changes in the slope, $d\varepsilon/dM_{\mathrm{sat}}$. Though ε has nonmagnetic contributions, the increase in ε upon entering region III suggests a predominance of the magnetic term. Thus, as the AFM background becomes more *C* type for $x>0.07$, with a lower free energy, there is an increased energy cost for the formation of FM clusters.

The results agree with qualitative arguments[19] predicting FM coupling of the isolated Mn^{3+} moments with their Mn^{4+} neighbors and the formation of multiple magnetic phases, however, a decrease of T_N is observed[20] for $x<0.1$ instead of the predicted increase. Calculations by de Gennes illustrate that a bound electron gives rise to a local distortion of the spin lattice leading to long-range canting of the AFM moments,[4] in contrast to the local ferromagnetism and mixed

phases suggested in these experiments. More detailed calculations reveal that canting is unstable in large regions of the $La(Ca)MnO_3$ phase diagram when the Hund's rule exchange energy $J_H < \infty$ (Ref. 21) and Coulomb repulsion is considered. Contemporary theories[1,6–10] agree that phase segregation is likely in isolated regions of the $La(Ca)MnO_3$ phase diagram. In the experimental region discussed above, calculations utilizing a one-orbital model (no Jahn-Teller effects) reveal phase segregation into FM and AFM regions and further work including Jahn-Teller effects (the two-orbital model) reveals phase segregation over a wide range of electron-phonon couplings.[7] Another study[10] finds phase segregation in the electron concentration regime of our experimental work, although an enhancement of T_N in regions **I** and **II** of Fig. 2(a) is suggested. Analytical calculations found phase segregation to occur in the range $0.5 < x < 1$,[8] however, the magnetic exchange of $LaMnO_3$ is AFM along the *c* axis and FM in the perpendicular direction therefore precluding direct comparison to magnetically isotropic (*G*-type) La-doped $CaMnO_3$. Another analytical investigation[9] finds that an increase in local magnetization causes an increase in local charge-carrier density resulting in potential wells for the carriers; spatial electron-density fluctuations lead to an unstable canted AFM state and phase segregation into FM and AFM regions. Our observations largely support these current theories[6–10,13,21] and, furthermore, establish detailed phase boundaries to fertilize future theoretical and experimental developments.

The results presented here suggest phase segregation resulting from the strong competition among local FM and long-range AFM order in a region of the $Ca(La)MnO_3$ phase diagram not previously studied in great detail and provide a simple alternative for the long-accepted scenario of canted AFM moments in electron-doped $CaMnO_3$. Moreover, electron-doped $CaMnO_3$ is revealed as a simple model system for future studies of phase segregation and FM polarons in transition-metal oxides.

The authors are indebted to E. Dagotto, D. Emin, D. Goodwin, W. Pickett, S. Oseroff, and Yi-Kuo Yu for valuable discussions. Partial support at FAU was provided through NSF Grant No. DMR-9982834. Work at the University of Miami was supported by NSF Grant No. DMR-9631236.

[1] B. Goss Levi, Phys. Today **51** (6), 19 (1998), and references therein.
[2] E. O. Wollan and W. C. Koehler, Phys. Rev. **100**, 545 (1955).
[3] W. Bao, J. D. Axe, C. H. Chen, S.-W. Cheong, P. Schiffer, and M. Roy, Physica B **241**, 418 (1998); W. Bao, J. D. Axe, C. H. Chen, and S.-W. Cheong, Phys. Rev. Lett. **78**, 543 (1997).
[4] P.-G. De Gennes, Phys. Rev. **118**, 141 (1960).
[5] M. Hennion, F. Moussa, G. Bitteau, J. Rodrîguez-Carvajal, L. Pinsard, and A. Revcolevschi, Phys. Rev. Lett. **81**, 1957 (1998).
[6] A. Moreo, S. Yunoki, and E. Dagotto, Science **283**, 2034 (1999), and references therein.
[7] S. Yunoki and A. Moreo, Phys. Rev. B **58**, 6403 (1998); S. Yunoki, A. Moreo, and E. Dagotto, Phys. Rev. Lett. **81**, 5612 (1998).
[8] D. P. Arovas and G. Guinea, Phys. Rev. B **58**, 9150 (1998); D. P. Arovas, G. Gómez-Santos, and F. Guinea, *ibid.* **59**, 13 569 (1999).
[9] E. L. Nagaev, Phys. Rev. B **58**, 2415 (1998).
[10] S.-Q. Shen and Z. D. Wang, Phys. Rev. B **58**, R8877 (1998).
[11] V. J. Emery, S. A. Kivelson, and H. Q. Lin, Phys. Rev. Lett. **64**, 475 (1990).
[12] J. A. M. van Roosmalen and E. H. P. Cordfunke, J. Solid State Chem. **110**, 109 (1994).
[13] D. Emin and M. S. Hillery, Phys. Rev. B **37**, 4060 (1988).
[14] H. Chiba, M. Kikuchi, K. Kusaba, Y. Muraoka, and Y. Syono, Solid State Commun. **99**, 499 (1996); I. O. Troyanchuk, N. V. Samsonenko, H. Szymezak, and A. Nabialek, J. Solid State Chem. **131**, 144 (1997); A. Maignan, C. Martin, F. Damay, B. Raveau, and J. Hejtmanek, Phys. Rev. B **58**, 2758 (1998).
[15] W. E. Pickett and D. J. Singh, Phys. Rev. B **53**, 1146 (1996).
[16] J. L. Cohn and J. J. Neumeier (unpublished).
[17] J. M. D. Coey and S. Von Molnar, Adv. Phys. **48**, 167 (1999).
[18] C. Rettori, D. Rao, J. Singley, D. Kidwell, S. B. Oseroff, M. T. Causa, J. J. Neumeier, K. J. McClellan, S.-W. Cheong, and S. Schultz, Phys. Rev. B **55**, 3083 (1997).
[19] J. B. Goodenough, Phys. Rev. **100**, 564 (1955).
[20] J. J. Neumeier and D. H. Goodwin, J. Appl. Phys. **85**, 5591 (1999).
[21] S. K. Mishra, S. Satpathy, F. Aryasetiawan, and O. Gunnarsson, Phys. Rev. B **55**, 2725 (1997).